How does the presence of a body affect the performance of an actuator disk?

de Oliveira Andrade, Gael; Balbino Dos Santos Pereira, Ricardo; Ragni, Daniele; Avallone, Francesco; van Bussel, Gerard

DOI
10.1088/1742-6596/753/2/022005

Publication date
2016

Document Version
Final published version

Published in
Journal of Physics: Conference Series

How does the presence of a body affect the performance of an actuator disk ?

2016 J. Phys.: Conf. Ser. 753 022005

(http://iopscience.iop.org/1742-6596/753/2/022005)

How does the presence of a body affect the performance of an actuator disk ?

G de Oliveira, R B Pereira, D Ragni, F Avallone, G van Bussel
Aerodynamics Department, Aerospace Faculty, TU Delft, Delft 2629HS, The Netherlands

Abstract. The article seeks to unify the treatment of conservative force interactions between axi-symmetric bodies and actuators in inviscid flow. Applications include the study of hub interference, diffuser augmented wind turbines and boundary layer ingestion propeller configurations. The conservation equations are integrated over infinitesimal streamtubes to obtain an exact momentum model contemplating the interaction between an actuator and a nearby body. No assumptions on the shape or topology of the body are made besides (axi)symmetry. Laws are derived for the thrust coefficient, power coefficient and propulsive efficiency. The proposed methodology is articulated with previous efforts and validated against the numerical predictions of a planar vorticity equation solver. Very good agreement is obtained between the analytical and numerical methods.

1. Introduction

Questions on the performance of actuator disks with nearby bodies arose at the dawn of rotor aerodynamics. Shrouded propellers gained popularity with the ideas of Coanda [1] and the pioneering work of Stipa [2] and Kort [3]. Only few concepts [4, 5] were put forward for aeronautical applications but shrouds are routinely used to improve the propulsive efficiency of maritime vessels [6, 7].

In the field of wind energy, shrouds were suggested to improve wind turbine performance by Betz himself [8]. The studies of Lilley [9] reignited interest on ducted windmills and continuous experimental efforts [10, 11] promoted reflexion on concentrator and diffuser systems. A significant body of literature emerged on the theory of Diffuser Augmented Wind Turbines [12–22].

The present contribution is meant to formalize the ideas of de Vries [12] for studying conservative force [23] interaction mechanisms between (axi)symmetric bodies and actuator disks. The article starts with the derivation of an exact momentum model for the performance of a single actuator disk with nearby bodies. Section 3 reverts the perspective to discuss the effect of the actuator on a collection of bodies. Section 4 interprets the power coefficient of an actuator-body system by complementing analytical predictions with numerical simulations. Finally, section 5 discusses the optimality of various actuator-body systems while framing the present results with previous efforts.

2. Model of Actuator with Nearby Body

Inspired by the seminal works of Betz [24] and Joukowski [25], the study focuses on the steady isentropic flow of inviscid incompressible fluids. All processes are governed by a simple form of the Euler equations complemented by the fundamental thermodynamic relation [26, 27]:

$$\begin{cases} (\boldsymbol{U}\cdot\nabla)\,\boldsymbol{U} = -\frac{1}{\rho}\nabla p + \frac{1}{\rho}\boldsymbol{f} \\ \nabla\cdot\boldsymbol{U} = 0 \end{cases} \quad , \qquad dh = TdS + \frac{1}{\rho}dp \quad with \quad dS \equiv 0$$

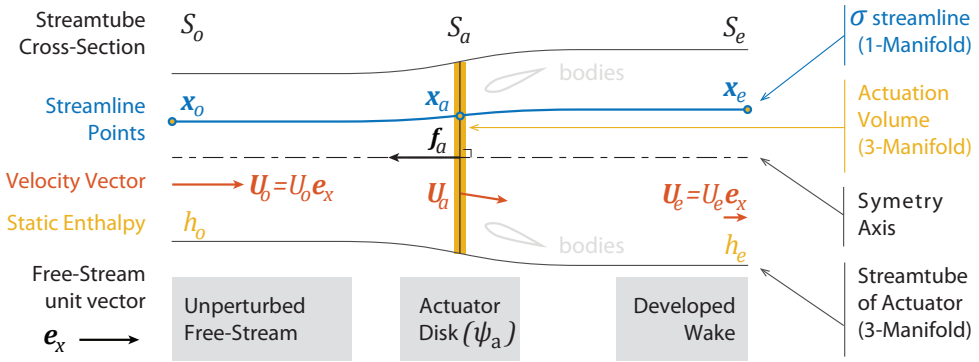

Figure 1. Flow Configuration and Nomenclature (wind turbine mode)

The specific internal energy ε of the fluid is constant and a simplified form of Crocco's theorem holds, written in terms of static h and total h^t enthalpy.

$$\left.\begin{array}{l} dS=0 \\ d\varepsilon=0 \end{array}\right\} \quad \Rightarrow \qquad \nabla h^t - \boldsymbol{U}\times\boldsymbol{\omega} = \frac{1}{\rho}\boldsymbol{f} \quad with \qquad \left\{\begin{array}{l} \boldsymbol{\omega}=\nabla\times\boldsymbol{U} \\ h^t = h + \frac{1}{2}(\boldsymbol{U}\cdot\boldsymbol{U}) \\ h = \varepsilon + \frac{p}{\rho} \end{array}\right.$$

Actuation surfaces are conceptuallized as the asymptotic equivalent of constant actuation volumes with vanishing thickness $t \to 0$. Pressure discontinuities accross actuator disks are seen as a consequence rather than a definition [23]. The disk $\psi_a \subset \mathbb{R}^3$ is a 2-manifold that exerts a constant force per unit surface $\boldsymbol{\phi}_a = \phi_a \boldsymbol{e}_x$ and its total force $\boldsymbol{F}_a$ corresponds to that of an equivalent actuation volume $\Omega_a \subset \mathbb{R}^3$, a 3-manifold that exerts a constant force per unit volume $\boldsymbol{f}_a = f_a \boldsymbol{e}_x$.

$$\psi_a \in \lim_{t\to 0} \Omega_a \qquad , \qquad \boldsymbol{F}_a = \int \boldsymbol{f}_a d\Omega_a = \int \boldsymbol{\phi}_a d\psi_a = F_a \boldsymbol{e}_x$$

The model comprises a free-stream $\boldsymbol{U}_o = U_o \boldsymbol{e}_x$, one or more finite bodies and a flat actuator disk ψ_a. Setups are either axisymmetric or planar. The symmetry axis (or plane) is aligned with the free-stream and contains the normal unit vector $\boldsymbol{n}_a = \boldsymbol{e}_x$ of the actuation surface.

The derivation starts by integrating Crocco's theorem along some streamline $\sigma \subset \mathbb{R}^3$ that crosses the actuator, as depicted in figure 1. The σ streamline is a $1-$manifold whose tangent unit vector $\boldsymbol{r}_\sigma = \boldsymbol{U}/|\boldsymbol{U}|$ facilitates the use of the fundamental theorem of multivariate calculus:

$$\underbrace{\int (\nabla h^t)\cdot \boldsymbol{r}_\sigma d\sigma}_{=h_e^t - h_o^t} = \frac{1}{\rho}\underbrace{\int \boldsymbol{f}\cdot\boldsymbol{r}_\sigma d\sigma}_{=\frac{\boldsymbol{U}_a\cdot\boldsymbol{\phi}_a}{\boldsymbol{U}_a\cdot\boldsymbol{n}_a}=\phi_a} + \underbrace{\int (\boldsymbol{U}\times\boldsymbol{\omega})\cdot\boldsymbol{r}_\sigma d\sigma}_{=0}$$

$$\Leftrightarrow \qquad h_e^t - h_o^t = \frac{\phi_a}{\rho} \qquad because \quad \boldsymbol{r}_\sigma \parallel \boldsymbol{U} \Rightarrow (\boldsymbol{U}\times\boldsymbol{\omega})\cdot\boldsymbol{r}_\sigma = 0$$

Wakes of inviscid incompressible flow can be transported to infinity, but static pressure and static enthalpy perturbations vanish asymptotically with distance [26]. The corollary is that the developped wake of a constant loading actuator is always homogeneous, irrespective of the presence of bodies:

$$\begin{aligned} \phi_a &= \rho\left(h_e + \frac{1}{2}U_e^2\right) - \rho\left(h_o + \frac{1}{2}U_o^2\right) \\ &= \frac{1}{2}\rho\left(U_e^2 - U_o^2\right) + \rho\underbrace{(h_e - h_o)}_{\to 0} = \frac{1}{2}\rho\left(U_e^2 - U_o^2\right) \qquad with \quad U_e = \left|\boldsymbol{U}_{(\boldsymbol{x}_e)}\right| \end{aligned} \tag{1}$$

For constant loading symmetric actuator-body configurations, it can be shown that the vanishing of pressure perturbations at infinity also implies that the terminal wake is aligned with the free-stream:

$$\boldsymbol{x}_e \in \psi_e \quad \Rightarrow \quad \left(\boldsymbol{U}_{(\boldsymbol{x}_e)} = U_e \boldsymbol{e}_x \quad \wedge \quad U_e \perp \boldsymbol{x}_e\right)$$

Momentum conservation can also be studied with path integrals along streamlines. The procedure is relatively unusual and builds upon the idea that the convective derivative corresponds to the projection of the velocity field on the velocity Jacobian:

$$\left(\boldsymbol{U}\cdot\nabla\right)\boldsymbol{U} = \left[J^{\boldsymbol{U}}\right]\boldsymbol{U} \qquad \Rightarrow \qquad \left[J^{\boldsymbol{U}}\right]\frac{\boldsymbol{U}}{|\boldsymbol{U}|} = -\frac{1}{\rho}\frac{\nabla p}{|\boldsymbol{U}|} + \frac{1}{\rho}\frac{\boldsymbol{f}}{|\boldsymbol{U}|}$$

In the above form, the system of Euler equations can be integrated along an arbitrary streamline σ with the fundamental theorem of multivariate calculus. The computation of the integral of the force term accross the actuator involves several intermediate steps that were deemed outside the scope of the present contribution:

$$\begin{aligned} \underbrace{\int \left(\left[J^{\boldsymbol{U}}\right]\frac{\boldsymbol{U}}{|\boldsymbol{U}|}\right) d\sigma}_{=\boldsymbol{U}_o - \boldsymbol{U}_e} &= -\frac{1}{\rho}\int \frac{\nabla p}{|\boldsymbol{U}|} d\sigma + \frac{1}{\rho}\underbrace{\int \frac{\boldsymbol{f}}{|\boldsymbol{U}|} d\sigma}_{=\frac{\boldsymbol{\phi}_a}{\boldsymbol{U}_a\cdot\boldsymbol{n}_a}} \\ \Leftrightarrow \qquad \boldsymbol{U}_{(\boldsymbol{x}_e)} - \boldsymbol{U}_{(\boldsymbol{x}_o)} &= -\frac{1}{\rho}\int \frac{\nabla p}{|\boldsymbol{U}|} d\sigma + \frac{1}{\rho}\frac{\boldsymbol{\phi}_a}{\boldsymbol{U}_{(\boldsymbol{x}_a)}\cdot\boldsymbol{n}_a} \end{aligned}$$

Conservation of momentum is entirely described by the streamwise component ($\boldsymbol{e}_x$) of the integrated equations, corresponding to the dot product of the free-stream unit vector $\boldsymbol{e}_x$ with the system of n equations:

$$U_e - U_o = -\frac{1}{\rho}\int \left(\frac{\nabla p}{|\boldsymbol{U}|}\cdot\boldsymbol{e}_x\right) d\sigma + \frac{1}{\rho}\frac{\phi_a}{\boldsymbol{U}_{(\boldsymbol{x}_a)}\cdot\boldsymbol{n}_a}$$

The total force exerted on the flow by the actuator is related with the velocity field by integrating the momentum conservation statement accross the actuation surface:

$$F_a = \int \phi_a d\psi_a = \int \rho\left(U_e - U_o\right)\boldsymbol{U}_{(\boldsymbol{x}_a)}\cdot\boldsymbol{n}_a d\psi_a + \int \left(\left(\int \frac{\nabla p}{|\boldsymbol{U}|}\cdot\boldsymbol{e}_x d\sigma\right)\boldsymbol{U}_{(\boldsymbol{x}_a)}\cdot\boldsymbol{n}_a\right) d\psi_a \tag{2}$$

Because the wake is homogeneous, the first parcel can be rewritten exactly in terms of the average normal speed over the actuator, $\bar{U}_a$:

$$\begin{aligned} \left(U_e - U_o\right)\perp\boldsymbol{x}_a \,,\, \forall \boldsymbol{x}_a \in \psi_a \quad \Rightarrow \quad & \int \rho\left(U_e - U_o\right)\boldsymbol{U}_{(\boldsymbol{x}_a)}\cdot\boldsymbol{n}_a d\psi_a = \rho\left(U_e - U_o\right)\bar{U}_a S_a \\ \text{with} \quad \bar{U}_a = \frac{\int \boldsymbol{U}_{(\boldsymbol{x}_a)}\cdot\boldsymbol{n}_a d\psi_a}{\int d\psi_a} \qquad & \text{and} \qquad S_a = \int d\psi_a \end{aligned}$$

The second parcel corresponds to the streamwise component of the resultant of pressure forces exerted on the flow crossing the actuator. It is denoted as F_b and its meaning is discussed in section 3.

$$F_a = \phi_a S_a = \rho S_a \bar{U}_a\left(U_e - U_o\right) + F_b \quad with \quad F_b = \int \left(\left(\int \frac{\nabla p}{|\boldsymbol{U}|}\cdot\boldsymbol{e}_x d\sigma\right)\boldsymbol{U}_{(\boldsymbol{x}_a)}\cdot\boldsymbol{n}_a\right) d\psi_a \tag{3}$$

Matching expression 1 with expression 3 leads to a closed solution for the average normal speed on the actuator $\bar{U}_a$ in terms of F_b and U_e:

$$\frac{1}{2}\rho\left(U_e^2 - U_o^2\right) = \rho\bar{U}_a\left(U_e - U_o\right) + \frac{1}{S_a}F_b \quad \Leftrightarrow \quad \bar{U}_a = \frac{1}{2}\left(U_e + U_o\right) - \frac{1}{2}\frac{U_o^2}{\left(U_e - U_o\right)}\frac{F_b}{\frac{1}{2}\rho S_a U_o^2} \tag{4}$$

Interpretation is more instinctive when restating results in terms of relative speeds and adimensional force coefficients:

$$C_{F_b} = \frac{F_b}{\frac{1}{2}\rho S_a U_o^2} \qquad C_{F_a} = \frac{F_a}{\frac{1}{2}\rho S_a U_o^2} = \frac{\phi_a}{\frac{1}{2}\rho U_o^2} = \left(u_e^2 - 1\right)$$
$$u_e = \frac{U_e}{U_o} = \sqrt{C_{F_a} + 1} \qquad \bar{u}_a = \frac{U_a}{U_o} = \frac{1}{2}\left(u_e + 1\right) - \frac{1}{2}\frac{C_{F_b}}{(u_e - 1)}$$

Finally, the rate of energy exchange between the actuator and the flow is written from the flow perspective:

$$P = \int \phi_a U_a \cdot \boldsymbol{n}_a d\psi_a = \bar{U}_a S_a \phi_a = \frac{1}{2}\rho \bar{U}_a S_a \left(U_e^2 - U_o^2\right) = \frac{1}{2}\rho U_o^3 S_a \bar{u}_a \left(u_e^2 - 1\right)$$

Leading to a compact expression for the power coefficient of the actuator-body system:

$$\begin{aligned} C_P = \frac{P}{\frac{1}{2}\rho U_o^3 S_a} &= \frac{1}{2}\left(u_e + 1\right)\left(\left(u_e^2 - 1\right) - C_{F_b}\right) \\ &= \frac{1}{2}\left(1 + \sqrt{C_{F_a} + 1}\right)\left(C_{F_a} - C_{F_b}\right) \end{aligned} \tag{5}$$

Negative values correspond to energy extraction (wind turbine mode) while propulsive configurations exhibit positive power coefficients. Removing the body ($C_{F_b} = 0$) recovers the classical result [24, 25]:

$$\left.\begin{array}{l} \bar{a} = (1 - \bar{u}_a) \\ \bar{u}_a|_{C_{F_b}=0} = \frac{1}{2}\left(u_e + 1\right) \end{array}\right\} \quad \Rightarrow \quad \begin{array}{ll} C_P|_{C_{F_b}=0} & = \frac{1}{2}\left(u_e + 1\right)\left(u_e^2 - 1\right) \\ & = 4a\left(1 - a\right)^2 \end{array}$$

Expression 5 is consistent with the results of De Vries [12] and Werle & Preszl [19]. The present derivation is exact: by following a different path with fewer assumptions it reinforces and unifies these earlier works.

3. Streamwise Force on Body

C_{F_b} and F_b represent the streamwise component of the resultant of pressure forces exerted on the flow by all objects but the actuator. The thrust of the actuator+body system T is defined as the sum of all streamwise forces exerted on the flow by the actuator F_a and the body F_b:

$$T = F_a + F_b \qquad , \qquad C_T = \frac{T}{\frac{1}{2}\rho U_o^2 S_a} = \frac{F_a + F_b}{\frac{1}{2}\rho U_o^2 S_a} = C_{F_a} + C_{F_b}$$

When no bodies are present in a free-space flow, F_b is zero because no objects other than the actuator are able to support flow forces:

$$\left.\begin{array}{r} \text{no bodies} \\ \text{actuator present} \end{array}\right\} \quad \Rightarrow \quad F_b = 0$$

Axisymmetric and two-dimensional steady-state inviscid incompressible flows are energy conservative in the absence of external volume force fields $\boldsymbol{f} = 0$. D'Alembert's paradox [31, 33] imposes that an axi-symmetric body generates no drag or thrust when placed alone in a conservative stream:

$$\left.\begin{array}{r} \text{axi-symmetric body present} \\ \text{no actuator} \end{array}\right\} \quad \Rightarrow \quad F_b = 0$$

But the presence of non-solenoidal force fields (like those representing an actuator disk) allows non-conservative energy exchanges with the flow. In this case, far-field boundary conditions can be altered with the presence of a wake, and d'Alembert's paradox ceases to apply [34]:

$$\left.\begin{array}{r} \text{axi-symmetric body present} \\ \text{actuator present} \end{array}\right\} \quad \Rightarrow \quad F_b \neq 0$$

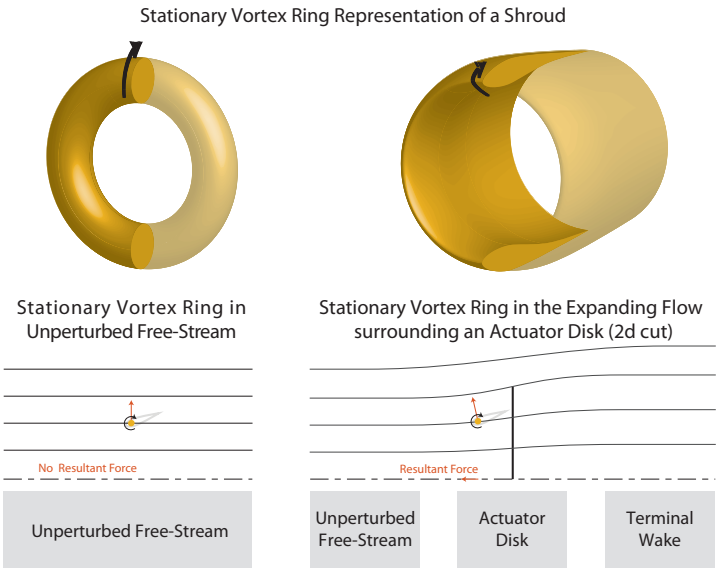

Figure 2. Shroud Analogy with Stationary (Bound) Vortex Ring

3.1. Inviscid force interactions and the resolution of D'Alembert's paradox

The action-reaction principle imposes that a momentum deficit (or superavit) appears in the flow whenever F_b is not zero [39].A non-zero momentum deficit implies the generation of a wake [26]. In viscous fluids, the wake feeds from the shear layers that form over bodies through the effect of skin friction, as in Saint Venant's resolution of d'Alembert's paradox [32]. But wakes do not need to be generated on the surfaces of the bodies that support streamwise forces, as noted by Biot [34].

Forces can be transmitted to the body by the pressure field, provided that a wake is created somewhere in the flow. The pressure field of a steady flow cannot accumulate energy but it can act as a transmission medium between bodies and wake generation elements: be they boundary layers [32], actuator disks or unsteady wakes [35, 36].

Wakes consist of non-vanishing far field velocity perturbations that invalidate the traditional proof of the Kutta-Joukowski theorem [26]. Steady variants of the Lagally theorem show that the local forces acting on a stationary vortex system are perpendicular to the bound vorticity vector and the local direction of the flow field [28, 29].

3.2. Shroud as stationary vortex ring

Airfoils are often represented as singular vortices in planar flow through Rayleigh's analogy [37]. In axisymmetric flow, an equivalent methaphor relates shrouds with stationary vortex rings [6, 38].

Figure 2 illustrates a stationary vortex ring placed alone in an unperturbed free-stream. For axisymmetric configurations, all local forces are contained in the ring plane and the resultant force is null. But if the ring has a non-zero angle of attack, lift and finite wing effects like induced drag appear, as exploited in Stipa's designs [2].

When a stationary vortex ring is placed in an expanding flow field, the forces acting on the stationary vortex ring cease to be contained in the ring plane. The ring exerts a thrust (or drag) that is either compensated by the generation of additional momentum deficit in an actuator wake or counteracted by other objects. In all cases, d'Alembert's paradox imposes that the sum of all pressure forces exerted on the collection of immersed objects is null if there are no wake generating devices [28, 34].

Just like a vortex ring in the decelerating flow field of an actuator disk, shrouds can sail in the flow surrounding a rotor operated in wind turbine or propeller mode. The importance of shroud forces is widely acknowledged [12, 14, 16–19] but its relation with d'Alembert's remains a topic of debate [35, 36].

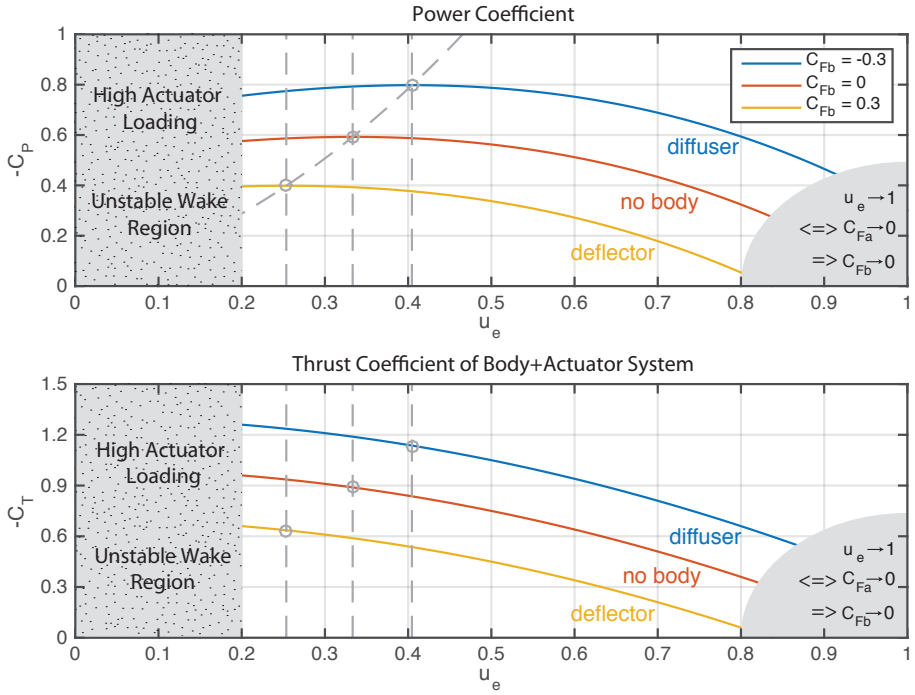

Figure 3. Thrust and Power Coefficient in Wind Turbine Mode

4. Performance of Actuator-Body System

4.1. Power Coefficient

The power coefficient law of equation 5 describes a surface in the (ue, C_{F_b}, C_P) space, of which three constant C_{F_b} cuts are presented in figure 3. The body force coefficient C_{F_b} is interpreted as a free parameter despite the fact that it must tend to zero when the actuator loading vanishes $C_{F_a} \to 0$ and a wake ceases to be generated $u_e \to 1$.

$$\begin{array}{lcl} C_{F_a} = 0 & \Leftrightarrow & u_e = 1 \\ C_{F_a} = 0 & \Rightarrow & C_{F_b} = 0 \\ C_{F_a} \neq 0 & \Rightarrow & C_{F_b} \text{ is a design parameter} \end{array} \tag{6}$$

The lower right corner of the C_P curves from figure 3 is therefore unreachable and shaded. The region of low terminal wake speeds $u_e < 0.2$ is also shaded to highlight that wake instabilities are likely to invalidate the theory for high actuator loadings [35, 36, 40].

4.2. Actuator-Body Configurations

It is well known [14, 16–18] that actuator-body systems can exhibit power coefficients above 16/27 when the body accelerates the flow and the actuator surface S_a is used as a reference. What deserves to be stressed is that the body does not need to surround the actuator to generate a concentrating force ($C_{F_b} < 0$). Numerical simulations illustrate this insight and contribute to the verification of analytical efforts.

Figure 4 shows the results of three numerical simulations conducted with a planar flow vorticity solver similar to the codes presented in references [20, 30, 38]. A flat actuator with diameter d and loading $C_{F_a} = 8/9$ is simulated together with a pair of symmetric counter-rotating vortices. The position of the singular vortex pair $\boldsymbol{x}_v = (x_v, \pm y_v)$ is varied while the circulation strenght Γ_v is kept constant. The circulation Γ_v of the vortex pair stays constant while its position $\boldsymbol{x}_v = (x_v, \pm y_v)$ across the three cases.

The numerical power coefficient C_P^{num} and body force coefficient $C_{F_b}^{num}$ are obtained by postprocessing the velocity field. The numerical interaction coefficient $C_{F_b}^{num}$ is combined with the prescribed actuator loading coefficient C_{F_a} to compute the theoretical power coefficient C_P^{theo} with expression 5.

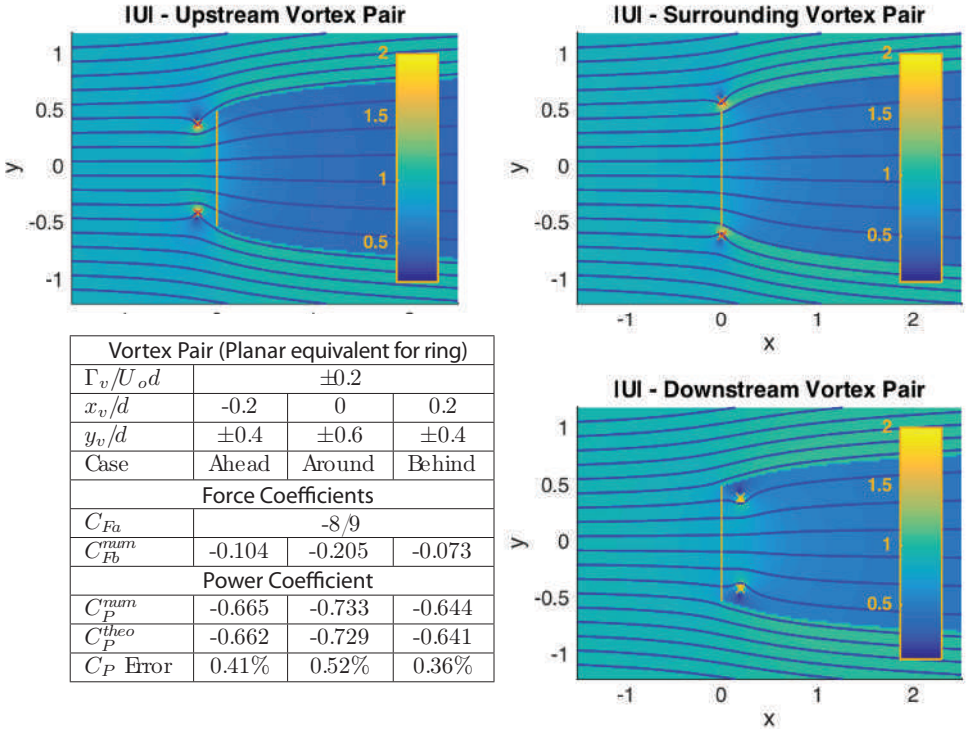

Vortex Pair (Planar equivalent for ring)			
$\Gamma_v/U_o d$		± 0.2	
x_v/d	-0.2	0	0.2
y_v/d	± 0.4	± 0.6	± 0.4
Case	Ahead	Around	Behind
Force Coefficients			
C_{Fa}		-8/9	
C_{Fb}^{num}	-0.104	-0.205	-0.073
Power Coefficient			
C_P^{num}	-0.665	-0.733	-0.644
C_P^{theo}	-0.662	-0.729	-0.641
C_P Error	0.41%	0.52%	0.36%

Figure 4. Comparison with Numerical Simulations for Three Particular Cases

Analytical and numerical predictions match to within half a percent, irrespective of the presence of a body. The placement of the vortex pair affects the actuator mass flow which determines power extraction (for a given actuator loading coefficient). A shrouding vortex ring yields the greatest power increase, but smaller upstream and downstream rings are also able to increase power extraction beyond the Betz limit.

4.3. Optimal Actuator Loading for Energy Extraction

The terminal wake speed for which energy extaction is maximized depends on the force that the body exerts on the flow. A simple extremum analysis of expression 5 defines the optimal terminal wake speed u_e^{opt} for any given body force coefficient C_{F_b}:

$$u_e^{opt}\big|_{C_{F_b}} \;:\; \frac{\partial}{\partial u_e}\left(C_P\right)\Big|_{C_{F_b}} = 0 \qquad \Rightarrow \qquad u_e^{opt}\big|_{C_{F_b}} = -\frac{1}{3}\left(1-\sqrt{4-3C_{F_b}}\right) \tag{7}$$

The existence of a bijection between u_e and C_{F_a} implies that the optimal actuator loading $C_{F_a}^{opt}$ also depends on the body force coefficient C_{F_b}, as plotted in figure 5:

$$C_{F_a}^{opt}\big|_{C_{F_b}} = \left(u_e^{opt}\big|_{C_{F_b}}\right)^2 - 1 \qquad , \qquad C_T^{opt} = \left(u_e^{opt}\big|_{C_{F_b}}\right)^2 - 1 + C_{F_b} \tag{8}$$

Expressions 7 and 8 contrast with earlier claims that the optimal loading of an actuator disk does not depend on the presence of a body [16–19].

Of previous studies promoting a universally optimal actuator loading coefficient of $-8/9^{ths}$, the approach of Werle & Preszl [19] is closest to the present methodology. They proposed a power coefficient law that is formally equivalent to expression 5 but written with different variables:

$$C_P = -\frac{1}{2}\left(1+C_s^{wp}\right)C_{F_a}^{wp}\left(1+\sqrt{1-C_{F_a}^{wp}}\right) \qquad , \quad C_s^{wp} \equiv -\frac{C_{F_b}}{C_{F_a}} = \frac{F_b}{F_a} \quad \wedge \quad C_{F_a}^{wp} \equiv -C_{F_a}$$

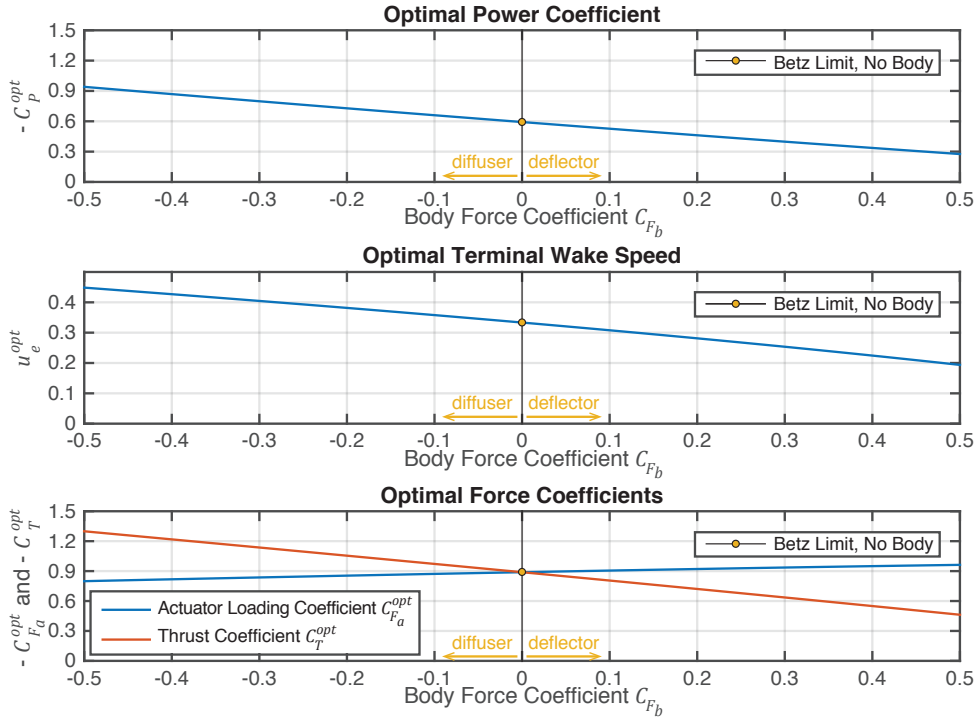

Figure 5. Optimal Loading of Actuator Disk with Nearby Body Exerting Constant Force on Flow

The use of a different adimensional coefficient to describe the body force C_s^{wp} lead to a different set of constrained optima:

$$C_{F_a}^{opt}\big|_{C_s^{wp}} \;:\; \frac{\partial}{\partial u_e}\left(C_P\right)\Big|_{C_s^{wp}} = 0 \qquad \Rightarrow \qquad C_{F_a}^{opt}\big|_{C_s^{wp}} = \frac{8}{9} \qquad \Rightarrow \qquad u_e^{opt}\big|_{C_s^{wp}} = \frac{1}{3}$$

A linear relation between C_{F_b} and C_{F_a} is implicitly assumed in this optimality regime. Only then does the optimal actuator loading coefficient correspond to $-8/9^{ths}$ despite the presence of a body. The assumption of a linear relation between C_{F_b} and C_{F_a} is a meaningful option, but not necessarily a universal one. Sorensen develops similar arguments in his recent review of wind turbine momentum theory [41].

4.4. Variation of Body Force with Actuator Loading

Figure 6 depicts a numerical study of the correlation between the body force coefficient C_{F_b} and the actuator force coefficient C_{F_a}. As for the numerical experiments of section 4.2, the setup consists of an actuator and a pair of counter rotating vortices in planar flow:

- The red lines depict the evolution of system parameters when the actuator loading C_{F_a} is varied while keeping the strenght $\Gamma_v/(U_o d)$ of the stationary vortex pair (ring) constant. Comparable behaviors can be achieved in real flows with Magnus effect lifting devices like Flettner rotors.
- The blue lines show the effect of actuator loading C_{F_a} on the body and actuator parameters when the strenght of the stationary vortex pair is adjusted to mimic the polar of flat plate with chord $c = 0.2d$ in straight flow. A real flat plate would exhibit a slightly different polar due to flow curvature effects [42], but the curves still provide reasonable qualitative insight on the interaction with small (low c/d) bodies.

The relation between force coefficients (C_{F_a} and C_{F_b}) is nearly linear when the strenght of the vortex pair is kept constant. Departures from linearity are subtle but noticeable for large actuator loading coefficients ($C_{F_a} > 6/9$).

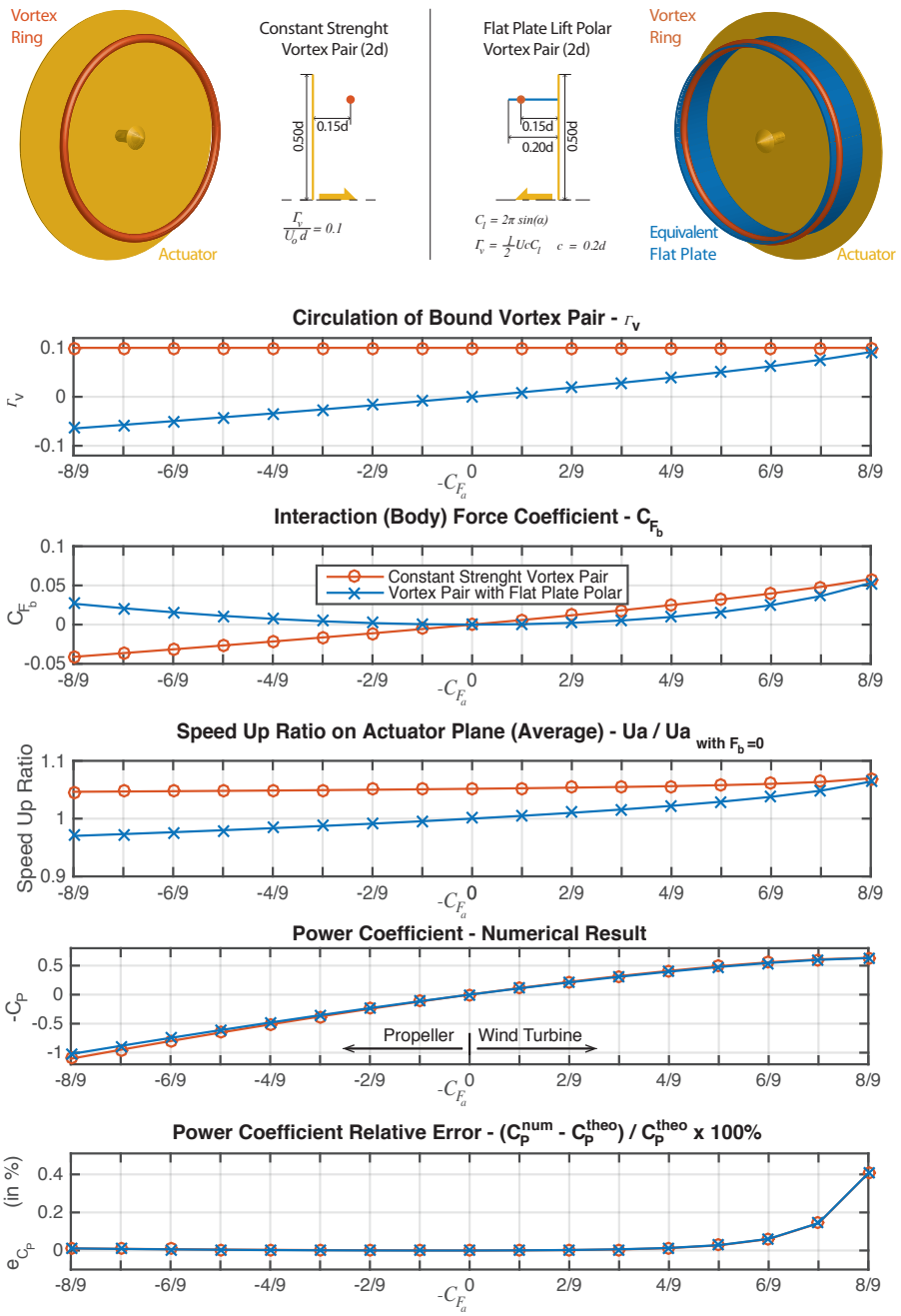

Figure 6. Effect of Actuator Loading on Body Force

The correlation between the C_{F_b} and C_{F_a} force coefficients is primarily quadratic when the strenght of the vortices grows with the angle of attack. Small angle approximations provide instinctive interpretations for this observation.

Actual relations between C_{F_a} and C_{F_b} are generally non-linear and depend on the specific type of body under consideration and its placement relative to the actuator disk. The choice of an optimal actuator loading coefficient depends on the correlation between the body force coefficient C_{F_b} and the actuator force coefficient C_{F_a}.

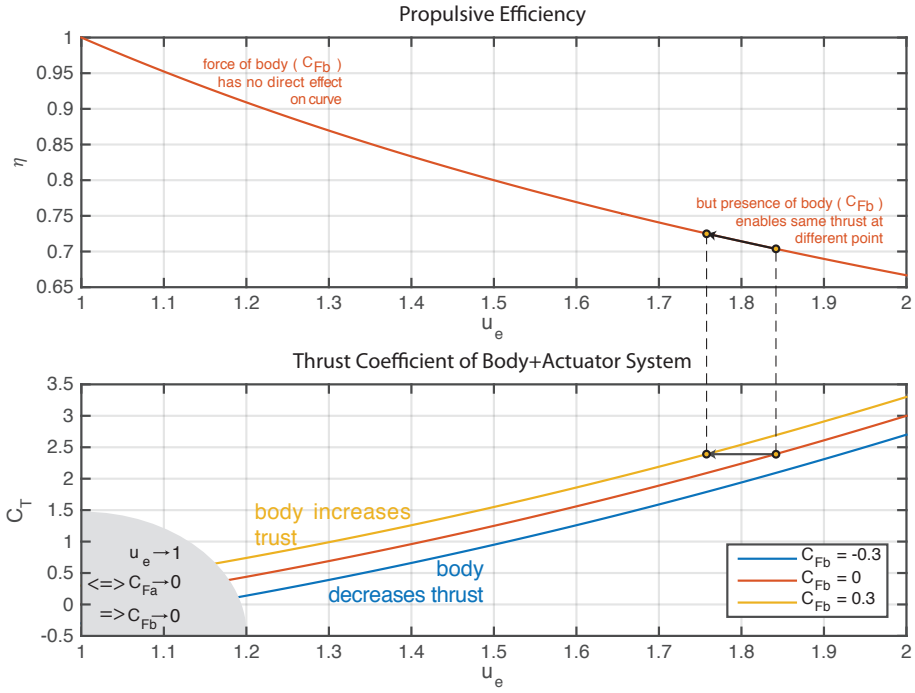

Figure 7. Thrust and Propulsive Efficiency for Actuator-Body System in Propeller Mode

4.5. Propulsive Efficiency

The propulsive efficiency η of the actuator-body system is defined as the ratio between the propulsive work U_oT and the power imparted to the fluid P:

$$\eta = \frac{U_oT}{P} = \frac{u_e^2-1+\xi}{\frac{1}{2}(u_e+1)(u_e^2-1+\xi)} = \frac{1}{\frac{1}{2}(u_e+1)} \tag{9}$$

The propulsive efficiency curve does not depend explicitly on the body force coefficient C_{F_b}. Still, the body can be used to achieve the same thrust C_T with a lower actuator load C_{F_a} and thereby improve propulsive efficiency in an indirect way [7].

5. Final Note

The study strenghtened the insight of de Vries [12], showing that in the steady state (axi)symmetric flow of inviscid incompressible fluids, conservative force interaction mechanisms between a body and an actuator disk:

- Influence the total thrust of an actuator-body system.
- Have no direct leverage on the propulsive efficiency curve of the complete system.
- Are able to increase the power coefficient even if the body fits in the actuator streamtube.
- Generally affect the actuator loading at which the optimal power coefficient is reached.

The methodology was verified against the numerical predictions of a planar flow solver of the vorticity equation. Agreement between analytical and numerical predictions was observed to numerical accuracy.

References

[1] Coanda H 1910 *Brevet d'Invention ONPF* France **416.541**
[2] Stipa L 1933 Stipa monoplane with Venturi fuselage. *Rivista Aeronautica* **IX** 7
[3] Kort L 1936 Combined device of a ship's propeller enclosed by a nozzle. *US Patent* **2,030,375**
[4] Vuillet A and Morelli F 1986 New aerodynamic design of the fenestron*Proc. 12th Eur. Rot. Forum*

[5] Johnson E N and Turbe M A 2006 Modeling, Control, and Flight Testing of a Small-Ducted Fan Aircraft *Journal of Guidance, Control, and Dynamics* **29** 4 769-79
[6] Oosterveld M W C 1970 *Wake Adapted Ducted Propellers* Phd Thesis (Delft: Delft University of Technology)
[7] Carlton J S 2007 *Marine Propellers and Propulsion, 2nd edition* (Oxford: Butterworth-Heinemann)
[8] Betz A 1929 Energieumsetzungen in Venturidusen *Die Naturwissenschaften* **10** 160-4
[9] Lilley G M and Rainbird W J 1956 *A preliminary Report on the Design and Performance of a Ducted Windmill* Report **102** (Cranfield: College of Aeronautics)
[10] Oman R A, Forema K M and Gilbert B L 1975 A Progress Report on the Diffuser Augmented Wind Turbine *Proc. 3rd Biennial Conf. and Workshop on Wind Energy Conversion Systems Washington DC* p. 826-829
[11] Igra O 1976 Design and Perf. of a Turbine Suitable for an Aerogenerator *Energy Conversion* **15** 143-151
[12] de Vries O 1979 *Fluid Dynamic Aspects of Wind Energy Conversion* AGARDograph 243 (Brussels: AGARD)
[13] Hansen M O L, Sorensen N N and Flay R G J 2000 Effect of placing a diffuser around a wind turbine *Wind Energ.* **3** 207-13
[14] van Bussel G J W 1999 An assessment of the performance of diffuser augmented wind turbines (DAWTs) *Proceedings of the 3d ASME/JSME Joint Fluids Conference San Francisco CA* FEDSM99-7830
[15] Phillips D G 2003 *An investigation on diffuser augmented wind turbine design* Phd Thesis (Univ. Auckland)
[16] van Bussel G J W 2007 The science of making more torque from wind: Diffuser experiments and theory revisited. *J. Phys.: Conf. Series* **75** 012002
[17] Jamieson P 2008 Beating Betz - Energy Extraction Limits in a Uniform Flow Field *EWEC 2008, Brussels* **1**
[18] Jamieson P 2008 Generalized limits for energy extraction in a linear constant velocity flow field *Wind Energ.* **11** 445-57
[19] Werle M J and Presz W M 2008 Ducted Wind/Water Turbines and Propellers Revisited *J. Prop. and Power* **24** 5 1146-50
[20] McLaren-Gow S, Jamieson P and Graham J M R 2013 An inviscid approach to ducted turbine analysis *Proc. Eur. Wind Energ. Conf. & Exh. 2013, Vienna* vol 1 p 931-38
[21] Bontempo R 2014 *The Nonlinear Actuator Disk Method as Applied to Open and Ducted Rotors* Phd Thesis (University of Naples Federico II)
[22] Hjort S and Larsen H 2015 Rotor Design for Diffuser Augmented Wind Turbines *Energies* **8** 10736-774
[23] van Kuik G A M, Micallef D, Herraez I, van Zuijlen A H and Ragni D 2014 The role of conservative forces in rotor aerodynamics *Journal of Fluid Mechanics* **750** 284-315
[24] Betz A 1920 Das Maximum der Theoretisch Ausnuetzung des Windes durch Windmotoren *Z. fur das ges. Turbinenwesen* **26** 307-9
[25] Joukowski N 1929 *Theorie tourbillonaire de l'helice propulsive* (Paris: Gauthier-Villars)
[26] Batchelor G K 1967 *An Introduction to Fluid Dynamics* (Cambridge: CUP)
[27] Greitzer E M, Tan C S and Graf M B 2004 *Internal Flow: Concepts and Applications* (Cambridge: CUP)
[28] Wu C T, Yang F L and Young D L 2012 *J. Fluid Mechanics* **698** 73-92
[29] Bai C Y, Li J and Wu Z M 2013 Explicit force formlulas for two dimensional potential flow with multiple bodies and multiple free vortices *Arxiv Physics, Fluid Dynamics* arXiv:**1304**.5311 [physics.flu-dyn]
[30] van Kuik G A M and Lignarolo L E M 2015 *Wind Energ.* doi:10.1002/we.1902
[31] Alembert J R 1768 *Paradoxe propose aux geometres sur la resistance des fluides* Opuscules Mathematiques **5** 35 132-138 (Paris: Chez David)
[32] Saint-Venant A B 1847 Memoire sur la theorie de la resistances des fluides. Solution du paradoxe propose par d'Alembert aux geometres. *Comptes rendus hebd. des seances de l'acad. des sciences* **24** 1 243-46
[33] Grimberg G, Pauls W and Frisch U 2008 Genesis of d'Alembert's paradox and analytical elaboration of the drag problem *Physica D: Nonlinear Phenomena* **237** 1878-86
[34] Biot M 1930 *L'hydrodynamique moderne et ses applications* Rev. des Quest. Scient. 9/30 235-257
[35] Birkhoff G 1950 *Hydrodynamics: a study in logic, fact and similitude* (Princeton: Princeton University Press)
[36] Hoffman J and Johnson C 2010 Resolution of dAlemberts Paradox *J. of Math. Fluid Mech.* **12** 3 321-34
[37] Hirschel E H, Prem H and Madelung G 2004 *Aeronautical Research in Germany* (Berlin: Springer Verlag)
[38] Falcao Campos J A C 1983 On the calculation of ducted propeller performance in axisymmetric flows *PhD Dissertation* Delft University of Technology
[39] Brederode V 2014 *Aerodinamica Incompressivel: Fundamentos* (Lisboa: IST Press)
[40] Glauert H 1926 General Theory of the Autogyro *Reports and Memoranda* **1111** British ARC
[41] Sorensen J N 2016 *General Momentum Theory for Horizonthal Axis Wind Turbines* (Springer International)
[42] Migliore P G, Wolfe W P and Fanucci J B 1980 Flow Curvature Effects on Darrieus Turbine Blade Aerodynamics *Journal of Energy* **4** 2 49-55